

# Tight-binding electronic spectra on graphs with spherical topology II: the effect of spin-orbit interaction

Y Avishai<sup>1,2,3,4</sup> and J M Luck<sup>3</sup>

<sup>1</sup> Department of Physics and Ilse Katz Center for Nanotechnology, Ben Gurion University, Beer Sheva 84105, Israel

<sup>2</sup> RTRA – Triangle de la Physique, Les Algorithmes, 91190 Saint-Aubin, France

<sup>3</sup> Institut de Physique Théorique<sup>‡</sup>, CEA Saclay, 91191 Gif-sur-Yvette cedex, France

<sup>4</sup> Laboratoire de Physique des Solides<sup>§</sup>, Université Paris-Sud, 91405 Orsay cedex, France

**Abstract.** This is the second of two papers devoted to tight-binding electronic spectra on graphs with the topology of the sphere. We investigate the problem of an electron subject to a spin-orbit interaction generated by the radial electric field of a static point charge sitting at the center of the sphere. The tight-binding Hamiltonian considered is a discretization on polyhedral graphs of the familiar form  $\mathbf{L} \cdot \mathbf{S}$  of the spin-orbit Hamiltonian. It involves  $SU(2)$  hopping matrices of the form  $\exp(i\mu \mathbf{n} \cdot \boldsymbol{\sigma})$  living on the oriented links of the graph. For a given structure, the dimensionless coupling constant  $\mu$  is the only parameter of the model. An analysis of the energy spectrum is carried out for the five Platonic solids (tetrahedron, cube, octahedron, dodecahedron and icosahedron) and the  $C_{60}$  fullerene. Except for the latter, the  $\mu$ -dependence of all the energy levels is obtained analytically in closed form. Rather unexpectedly, the spectra are symmetric under the exchange  $\mu \leftrightarrow \Theta - \mu$ , where  $\Theta$  is the common arc length of the links. For the symmetric point  $\mu = \Theta/2$ , the problem can be exactly mapped onto a tight-binding model in the presence of the magnetic field generated by a Dirac monopole, studied recently. The dependence of the total energy at half filling on  $\mu$  is investigated in all examples.

PACS numbers: 71.70.Ej, 73.22.-f, 73.20.-r, 73.20.At

E-mail: yshai@bgu.ac.il, jean-marc.luck@cea.fr

<sup>‡</sup> URA 2306 of CNRS

<sup>§</sup> UMR 9502 of CNRS

## 1. Introduction

The analogy between quantum dots and natural atoms is rather appealing, and in many cases quantum dots are referred to as artificial atoms (or molecules) [1]. Within the physics of low-dimensional electronic systems, quantum dots and natural molecules realize the ultimate extreme of zero dimension. So far, most investigations have been focused either on planar quantum dots or on quantum dots which occupy a small volume (quantum box or cavity). A novel class of zero-dimensional systems which so far has not received much attention is realized when electrons are confined to move on a compact surface of nanoscopic size. The simplest class of such surfaces has the topology of the sphere. An electron hopping between carbon atoms of a  $C_{60}$  fullerene (or its derivatives) provides the most natural candidate for such systems.

In the companion work [2] we have investigated in detail the spectra of tight-binding electrons moving on polyhedral graphs with spherical topology, subject to the radial magnetic field produced by a quantized magnetic charge. This problem was solved for the five Platonic solids (tetrahedron, cube, octahedron, dodecahedron, icosahedron), the  $C_{60}$  fullerene and a couple of less symmetric objects (diamonds and prisms). The main goal of the present work is to pursue this idea further by including the electron spin and taking into account the spin-orbit interaction. Within the same framework as in [2], the single-particle energy spectrum of an electron subject to a radial electric field which generates a Rashba-type spin-orbit interaction [3] is studied for the five platonic solids and the  $C_{60}$  fullerene.

The spin-orbit interaction is known to have a profound impact in atomic, nuclear and solid-state physics. Confining our discussion to the latter field, a dramatic example of its effect is the occurrence of an Anderson metal-insulator transition in disordered two-dimensional electronic systems [4]. Recall that the spin-orbit interaction emerges as a natural consequence of the Dirac equation, when the low-energy sector is described by the Pauli equation, and relativistic corrections are taken into account by means of a systematic  $1/c^2$  expansion [5]. For an electron of mass  $m$  and charge  $-e$ , subject to an electrostatic potential  $V(\mathbf{r})$ , and therefore to a static electric field  $\mathbf{E}(\mathbf{r}) = -\nabla V(\mathbf{r})$ , the spin-orbit term in the effective Hamiltonian is

$$\hat{\mathcal{H}}_{\text{SO}} = \frac{e\hbar}{8m^2c^2} (\mathbf{p} \cdot (\mathbf{E} \times \boldsymbol{\sigma}) + (\mathbf{E} \times \boldsymbol{\sigma}) \cdot \mathbf{p}), \quad (1.1)$$

where  $\mathbf{p} = -i\hbar\nabla$  is the momentum operator and  $\boldsymbol{\sigma}$  is the vector of Pauli matrices, so that  $\mathbf{S} = \hbar\boldsymbol{\sigma}/2$  is the electron spin operator. If the electrostatic potential  $V(\mathbf{r}) = V(r)$  is *central*, the spin-orbit Hamiltonian (1.1) simplifies to

$$\hat{\mathcal{H}}_{\text{SO}} = \frac{e}{2m^2c^2r} \frac{dV(r)}{dr} \mathbf{L} \cdot \mathbf{S}, \quad (1.2)$$

where  $\mathbf{L}$  is the electron orbital angular momentum operator. In particular, if the electron is confined to move on a spherical shell with radius  $R$ , the spin-orbit Hamiltonian (1.2) acquires the familiar form

$$\hat{\mathcal{H}}_{\text{SO}} = C\mathbf{L} \cdot \mathbf{S} = \frac{C}{2}(\mathbf{J}^2 - \mathbf{L}^2 - \mathbf{S}^2), \quad (1.3)$$

where  $C$  is a constant and  $\mathbf{J} = \mathbf{L} + \mathbf{S}$  is the total angular momentum.

The present work will be focused on the example of the Coulomb potential produced by a static electric charge  $q$  placed at the center of the sphere,

$$V(r) = \frac{q}{r}, \quad \mathbf{E}(r) = \frac{q\mathbf{r}}{r^3}. \quad (1.4)$$

For this potential, one has

$$C = -\frac{qe}{2m^2c^2R^3}. \quad (1.5)$$

For the sake of completeness, we present at the end of Section 2.1 a discussion of the order of magnitude of the spin-orbit interaction, although this can be found in many textbooks.

The Hamiltonian (1.3) has two eigenvalues  $E_{\pm}$ , respectively corresponding to the vectors  $\mathbf{L}$  and  $\mathbf{S}$  being parallel and antiparallel. If  $\ell = 0, 1, 2, \dots$  denotes the orbital quantum number, the eigenvalues  $E_{\pm}$  and their multiplicities  $m_{\pm}$  read

$$\begin{aligned} E_+ &= \frac{C\hbar^2\ell}{2}, & m_+ &= 2(\ell + 1), \\ E_- &= -\frac{C\hbar^2(\ell + 1)}{2}, & m_- &= 2\ell. \end{aligned} \quad (1.6)$$

This spectrum is not an even function of the coupling constant  $C$ , except in the classical regime, i.e., in the  $\ell \rightarrow \infty$  limit. This lack of a symmetry is expected on physical grounds. In the Coulomb case,  $C$  is indeed proportional to the product  $qe$  of both charges. Charges of the same sign ( $C < 0$ ) and charges of opposite signs ( $C > 0$ ) indeed correspond to physically distinct situations, which are not related by any symmetry. Furthermore, the situations where  $\mathbf{L}$  and  $\mathbf{S}$  are parallel and antiparallel are also known to exhibit different features, e.g. in scattering theory [6].

Our main objective is to construct and study natural discretizations of the spin-orbit Hamiltonian (1.3), within a tight-binding model where the electron lives on the sites (vertices) of a polyhedral graph drawn on the unit sphere and executes nearest-neighbor hopping. Our analysis will be based on an analogy with the more conventional situation of tight-binding (spinless) electrons subject to a given magnetic field  $\mathbf{B}(\mathbf{r}) = \nabla \times \mathbf{A}(\mathbf{r})$ . In this case, the hopping of particles from site A to site B is described by a hopping term of the form  $a_A^\dagger U_{AB} a_B + \text{h.c.}$  in the tight-binding Hamiltonian, where  $U_{AB}$  is a phase factor, i.e., an element of the Abelian gauge group  $U(1)$ . It is generally accepted that the following expression, known as the Peierls substitution [7], is an appropriate choice:

$$U_{AB} = \exp \left\{ \frac{ie}{\hbar c} \int_{\gamma(A,B)} \mathbf{A} \cdot d\mathbf{r} \right\}, \quad (1.7)$$

where  $\gamma(A, B)$  is a given continuous path joining site A to site B. The phase factor so defined depends in general on the whole path  $\gamma(A, B)$ , and not only on the endpoints A and B (see [8] and [9] for recent investigations related to this matter). For the present problem involving the non-Abelian gauge group  $SU(2)$ , the construction of the hopping terms requires some extra care. Indeed, since  $SU(2)$  matrices do not commute among themselves, an ordering prescription is needed in general.

The setup of the present paper is the following. The model is introduced in Section 2.1. The hopping matrices  $U_{AB}$ , which are elements of the non-Abelian  $SU(2)$  gauge group, are evaluated for the two natural choices of shortest paths, the straight line segment and the arc of a great circle. A unique dimensionless parameter  $\mu$  then appears in a natural way. The main properties of the model, and especially its symmetries, are studied in Section 2.2. In Section 3 the five regular polyhedra or Platonic solids and the  $C_{60}$  fullerene (modeled as a regular truncated icosahedron) are investigated in detail. The spectra of the tight-binding Hamiltonian are respectively determined in Sections 3.1 to 3.6. The total energy at half filling is studied in Section 4, whereas Section 5 contains a short discussion.

## 2. The model

### 2.1. Definitions

In this work we consider a tight-binding model defined on polyhedral graphs drawn on the unit sphere. We denote by  $V$  the number of vertices (sites), by  $L$  the number of links (bonds) and by  $F$  the number of faces of a polyhedron. In the present case of spherical topology, the Euler relation reads (see e.g. [10])

$$V - L + F = 2. \quad (2.1)$$

In all the polyhedra considered in the following, all the links have equal arc length  $\Theta$  (with  $0 < \Theta < \pi$ ). For any pair of neighboring vertices A and B, we thus have

$$\mathbf{A} \cdot \mathbf{B} = \cos \Theta, \quad \mathbf{A} \times \mathbf{B} = \mathbf{n}_{AB} \sin \Theta, \quad (2.2)$$

where  $\mathbf{A}$  is the unit vector joining the center of the sphere to A, and so on, whereas  $\mathbf{n}_{AB}$  is the consistently oriented unit vector perpendicular to  $\mathbf{A}$  and  $\mathbf{B}$ , so as to have

$$\mathbf{n}_{AB} = -\mathbf{n}_{BA}. \quad (2.3)$$

The tight-binding model is defined by means of the Hamiltonian

$$\hat{\mathcal{H}} = \sum_{\langle AB \rangle} \left( \mathbf{a}_A^\dagger U_{AB} \mathbf{a}_B + \text{h.c.} \right), \quad (2.4)$$

where the sum runs over the  $L$  oriented links  $\langle AB \rangle$  of the polyhedron, whereas

$$\mathbf{a}_A^\dagger = (a_{A\uparrow}^\dagger, a_{A\downarrow}^\dagger), \quad \mathbf{a}_A = \begin{pmatrix} a_{A\uparrow} \\ a_{A\downarrow} \end{pmatrix}, \quad (2.5)$$

where  $a_{A\sigma}^\dagger$  and  $a_{A\sigma}$  are respectively the creation and annihilation operators of an electron at site A with spin component  $\sigma = \uparrow$  or  $\downarrow$ , and the matrices  $U_{AB}$  are elements of the non-Abelian gauge group  $SU(2)$ , i.e.,  $2 \times 2$  unitary matrices with unit determinant, describing the spin-orbit coupling on an electron hopping from site A to a neighboring site B.

In analogy with the Abelian case described by the Peierls substitution (1.7), the  $SU(2)$  matrix  $U_{AB}$  is expressed as a path-ordered integral:

$$U_{AB} = \text{P exp} \left\{ -ig \int_{\gamma(A,B)} (\mathbf{E} \times \boldsymbol{\sigma}) \cdot d\mathbf{r} \right\}, \quad (2.6)$$

where  $\gamma(A, B)$  is a given path joining site A to site B, and  $\mathbf{E}$  is the static electric field, as in (1.1).

The value of the coupling constant,

$$g = \frac{e}{4mc^2}, \quad (2.7)$$

is determined along the line of thought used in deriving the Peierls substitution in the Abelian case [7], and already considered e.g. in [11] in the case of the SU(2) group. The basic idea is to consider the spin-orbit term (1.1) as a perturbation of the free non-relativistic Hamiltonian  $\hat{\mathcal{H}}_0 = \mathbf{p}^2/(2m)$  and to use the approximation

$$\begin{aligned} \hat{\mathcal{H}}_0 + \hat{\mathcal{H}}_{\text{SO}} &= \frac{\mathbf{p}^2}{2m} + \frac{e\hbar}{8m^2c^2} (\mathbf{p} \cdot (\mathbf{E} \times \boldsymbol{\sigma}) + \text{h.c.}) \\ &\approx \frac{1}{2m} \left( \mathbf{p} + \frac{e\hbar}{4mc^2} \mathbf{E} \times \boldsymbol{\sigma} \right)^2 = -\frac{\hbar^2}{2m} \left( \nabla + i \underbrace{\frac{e}{4mc^2}}_g \mathbf{E} \times \boldsymbol{\sigma} \right)^2. \end{aligned} \quad (2.8)$$

The expressions inside parentheses in the second line are respectively the SU(2) covariant momentum and derivative [11]. It is worth noticing that the term obtained by expanding the square, i.e.,  $g^2\hbar^2\mathbf{E}^2/(2m)$ , if not neglected, is a scalar potential which does not affect the spin physics anyhow.

The present work is restricted to the situation where  $\mathbf{E}$  is the electric field generated by a static charge  $q$  sitting in the center of the sphere, given by (1.4), so that

$$(\mathbf{E} \times \boldsymbol{\sigma}) \cdot d\mathbf{r} = -\frac{q}{r^3} (\mathbf{r} \times d\mathbf{r}) \cdot \boldsymbol{\sigma}. \quad (2.9)$$

Let us now make the hypothesis that the path  $\gamma(A, B)$  is planar, i.e., entirely contained in the OAB plane. In this case, at every point of the path the infinitesimal vector  $\mathbf{r} \times d\mathbf{r}$  is perpendicular to the latter plane, i.e., aligned with the vector  $\mathbf{n}_{\text{AB}}$  introduced in (2.2). As a consequence, the path-ordering prescription is not needed, and (2.6) can be recast as

$$U_{\text{AB}} = \exp \left\{ igq \left( \int_{\gamma(A, B)} \frac{\mathbf{r} \times d\mathbf{r}}{r^3} \right) \cdot \boldsymbol{\sigma} \right\}. \quad (2.10)$$

There are two natural choices for the path  $\gamma(A, B)$ :

*Straight-line path.* If  $\gamma(A, B)$  is the shortest path in three-dimensional space, i.e., the straight line segment joining the points A and B,  $\mathbf{r}$  can be parametrized as

$$\mathbf{r} = (1-t)\mathbf{A} + t\mathbf{B} \quad (0 \leq t \leq 1). \quad (2.11)$$

We have then

$$\mathbf{r} \times d\mathbf{r} = \sin \Theta \mathbf{n}_{\text{AB}} dt, \quad r = (1 - 4 \sin^2(\Theta/2) t(1-t))^{1/2}, \quad (2.12)$$

so that (2.10) yields

$$U_{\text{AB}} = \exp(igq \sin \Theta I(\Theta) \mathbf{n}_{\text{AB}} \cdot \boldsymbol{\sigma}), \quad (2.13)$$

with

$$I(\Theta) = \int_0^1 \frac{dt}{(1 - 4 \sin^2(\Theta/2) t(1-t))^{3/2}} = \frac{1}{\cos^2(\Theta/2)}, \quad (2.14)$$

i.e.,

$$U_{AB} = \exp(2igq \tan(\Theta/2) \mathbf{n}_{AB} \cdot \boldsymbol{\sigma}). \quad (2.15)$$

*Great-circle path.* If  $\gamma(A, B)$  is the shortest path on the sphere, i.e., the arc of the great circle passing through A and B,  $\mathbf{r}$  can be parametrized as

$$\mathbf{r} = \frac{\sin(\Theta - \tau) \mathbf{A} + \sin \tau \mathbf{B}}{\sin \Theta} \quad (0 \leq \tau \leq \Theta). \quad (2.16)$$

We have  $r = 1$ , whereas

$$\mathbf{r} \times d\mathbf{r} = \mathbf{n}_{AB} d\tau, \quad (2.17)$$

so that (2.10) yields

$$U_{AB} = \exp(igq\Theta \mathbf{n}_{AB} \cdot \boldsymbol{\sigma}). \quad (2.18)$$

For both choices of the path  $\gamma(A, B)$ , Equations (2.15) and (2.18) yield the same expression for the SU(2) matrix  $U_{AB}$ :

$$U_{AB} = \exp(i\mu \mathbf{n}_{AB} \cdot \boldsymbol{\sigma}) = \cos \mu + i \sin \mu \mathbf{n}_{AB} \cdot \boldsymbol{\sigma}, \quad (2.19)$$

which gives the desired discretization of the familiar spin-orbit operator  $\mathbf{L} \cdot \mathbf{S}$  recalled in (1.3). The fact that the hopping matrix  $U_{AB}$  involves a vector parallel to  $\mathbf{A} \times \mathbf{B}$  was already noticed in the case of a Rashba spin-orbit interaction in semiconductors [12, 13].

For a given polyhedron, the model therefore has one single parameter, the dimensionless coupling constant  $\mu$ . Re-inserting for a while the physical radius  $R$  of the sphere, and using the expression (2.7) of the coupling constant  $g$ , we are left with the following expression for  $\mu$ , for both choices of the path  $\gamma(A, B)$ :

$$\mu = \varepsilon \times \begin{cases} 2 \tan(\Theta/2) & (\text{straight-line path}), \\ \Theta & (\text{great-circle path}), \end{cases} \quad (2.20)$$

with

$$\varepsilon = \frac{gq}{R} = -\frac{mR^2C}{2} = \frac{qe}{4mc^2R}. \quad (2.21)$$

The dimensionless (positive or negative) number  $\varepsilon$  gives a measure of the strength of the spin-orbit interaction. Its expression (2.21) can be made more transparent by introducing the (positive or negative) atomic number  $Z$ , such that the charge at the center of the sphere is  $q = Ze$ . One has then

$$\varepsilon = \frac{Z\alpha^2}{4} \frac{a_0}{R}, \quad (2.22)$$

where  $\alpha = e^2/(\hbar c) \approx 1/137$  is the fine structure constant and  $a_0 = \hbar^2/(me^2)$  is the Bohr radius, whereas  $R$  is the radius of the spherical sample. Although the number  $\varepsilon$  is a priori very small, due to the factor  $\alpha^2 \sim 10^{-4}$ , it is allowed to become appreciable in the following two ways. First, there is a priori no upper limit on the value of  $Z$ , as the charge  $q = Ze$  is treated in this work as a static classical charge. Second, spin-orbit interactions can be many orders of magnitude larger in solid materials than in vacuum, due to Bloch electrons moving close to atomic nuclei with relativistic velocities [14].

The dependence of the parameter  $\mu$  on the angle  $\Theta$  in (2.20) also deserves a word of comment. The same linear growth at small angles, i.e.,  $\mu \approx \varepsilon\Theta$ , holds for both paths, in accord with the expectation that we are dealing with a bona fide discretization of the familiar spin-orbit Hamiltonian (1.3). On the contrary, the regime of large angles ( $\Theta \rightarrow \pi$ ) exhibits two very different kinds of behavior:  $\mu$  remains finite in this limit in the case of a great-circle path, whereas it diverges in the case of a straight-line path, as the latter passes very near the center of the sphere, where the electric field becomes infinitely large.

Throughout the following, we shall adopt the theoretical viewpoint of considering  $\mu$  as an arbitrary parameter, forgetting both about its physical origin and about its expression (2.20). Of course, the arc length  $\Theta$  of the links is bound to keep its value, dictated by the geometry of the graph under consideration. The dependence of energy spectra on  $\mu$  will be investigated systematically, starting with a study of its symmetries in the next section.

## 2.2. Properties

We now turn to a discussion of various properties of the tight-binding Hamiltonian  $\hat{\mathcal{H}}$  of the problem, defined in (2.4), where the  $SU(2)$  matrices  $U_{AB}$  are given by (2.19), putting a special emphasis onto symmetries.

*Hermitian matrix representation.* The relation (2.3) ensures that the matrices  $U_{AB}$  obey

$$U_{AB} = U_{BA}^{-1} = U_{BA}^\dagger. \quad (2.23)$$

The Hamiltonian  $\hat{\mathcal{H}}$  is therefore represented by a  $2V \times 2V$  Hermitian matrix  $\mathcal{H}$ , whose rows and columns are labeled by a couple  $(A\sigma)$  where  $A = 1, \dots, V$  denotes a site and  $\sigma = \uparrow$  or  $\downarrow$  is a spin index, such that

$$\mathcal{H}_{(A\sigma)(B\tau)} = (U_{AB})_{\sigma\tau}. \quad (2.24)$$

The equation for the energy eigenvalues  $E_a$ , labeled by the integer  $a = 1, \dots, 2V$ , and the corresponding eigenfunctions  $\psi_{A,a}$  reads

$$E_a \psi_{A,a} = \sum_{B(A)} U_{AB} \psi_{B,a}, \quad (2.25)$$

where  $B(A)$  runs over the neighbors of  $A$ . More explicitly,

$$E_a \psi_{A\sigma,a} = \sum_{B(A)} \sum_{\tau=\uparrow,\downarrow} (U_{AB})_{\sigma\tau} \psi_{B\tau,a}. \quad (2.26)$$

*Sum rules.* The spectrum of the Hamiltonian  $\hat{\mathcal{H}}$  obeys the following sum rules

$$\sum_a E_a = 0, \quad \sum_a E_a^2 = 4L. \quad (2.27)$$

where the sums run over the  $2V$  eigenvalues  $E_a$ , repeated according to their multiplicities. The first sum equals  $\text{tr } \mathcal{H} = \sum_A \text{tr } U_{AA} = 0$ . This sum rule is a common feature to all tight-binding Hamiltonians with only non-diagonal matrix elements. The second sum equals  $\text{tr } \mathcal{H}^2 = \sum_{AB} \text{tr}(U_{AB}U_{BA}) = 4L$ . Equation (2.23) indeed implies that each

link  $\langle AB \rangle$  gives two contributions equal to  $\text{tr}(U_{AB}U_{AB}^\dagger) = \text{tr} \mathbf{1} = 2$ , i.e., the number of spin degrees of freedom.

*Kramers degeneracy.* All the energy levels of the Hamiltonian  $\hat{\mathcal{H}}$  are at least twofold degenerate, because of time-reversal symmetry, embodied in the Kramers theorem [15, 16]: if  $\psi_{A,a}$  is a solution of (2.25), another independent solution of the same equation, with the same energy  $E_a$ , is provided by the spinor  $\psi_{A,a}^{(K)}$ , where

$$\psi^{(K)} = i\sigma_y \psi^*, \quad \text{i.e.,} \quad \begin{cases} \psi_\uparrow^{(K)} = -\psi_\downarrow^*, \\ \psi_\downarrow^{(K)} = \psi_\uparrow^*. \end{cases} \quad (2.28)$$

Here and throughout the following, the star denotes complex conjugation.

*Homogeneous modes on regular polyhedra.* In the case of the five regular polyhedra, one can predict the existence of a twofold degenerate eigenvalue associated with homogeneous modes. Using the expression (2.19) of the matrices  $U_{AB}$ , the eigenvalue equation (2.25) can be recast as

$$E\psi_A = \sum_{B(A)} (\cos \mu + i \sin \mu \mathbf{n}_{AB} \cdot \boldsymbol{\sigma}) \psi_B. \quad (2.29)$$

For each site A, consider the vector

$$\mathbf{W}_A = \mathbf{A} \times \sum_{B(A)} \mathbf{B} = \sin \Theta \sum_{B(A)} \mathbf{n}_{AB}. \quad (2.30)$$

In the case of a regular polyhedron, one has  $\mathbf{W}_A = \mathbf{0}$  by symmetry. Indeed,  $\mathbf{W}_A$  is perpendicular to  $\mathbf{A}$ , and in the plane perpendicular to  $\mathbf{A}$  it has the  $p$ -fold rotational symmetry of the polyhedron, where  $p$  is the coordination number of the vertices.  $\mathbf{W}_A$  therefore clearly vanishes. As a consequence, (2.29) shows that the homogeneous wavefunction  $\psi_A = \chi$ , where  $\chi$  is a constant spinor, independent of the site A, is an eigenfunction of the Hamiltonian  $\hat{\mathcal{H}}$ . The corresponding twofold degenerate energy is  $E = p \cos \mu$ .

*Semi-periodicity.* The matrices  $U_{AB}$  given in (2.19) obey  $U_{AB}(\mu + \pi) = -U_{AB}(\mu)$ . The energy eigenvalues therefore obey the same property, referred to as *semi-periodicity*: they are changed into their opposites if  $\mu$  is changed to  $\mu + \pi$ . It is also worth noticing that the spectrum of the Hamiltonian  $\hat{\mathcal{H}}$  is not an even function of  $\mu$ , in spite of the identity  $U_{AB}(-\mu) = U_{AB}^\dagger(\mu)$ . This lack of symmetry has already been emphasized in the simpler example of the spin-orbit Hamiltonian (1.3).

$\mu \leftrightarrow \Theta - \mu$  *symmetry.* The Hamiltonian  $\hat{\mathcal{H}}$  has the following less obvious symmetry. For each site A, consider the spin operator in the direction of  $\mathbf{A}$ ,

$$S_A = \mathbf{A} \cdot \boldsymbol{\sigma}. \quad (2.31)$$

One has clearly  $S_A^2 = 1$ . Furthermore, using the identity

$$(\mathbf{a} \cdot \boldsymbol{\sigma})(\mathbf{b} \cdot \boldsymbol{\sigma}) = \mathbf{a} \cdot \mathbf{b} + i(\mathbf{a} \times \mathbf{b}) \cdot \boldsymbol{\sigma}, \quad (2.32)$$

one can check that

$$U_{AB}(\Theta) = S_A S_B \quad (2.33)$$

for any pair of neighboring vertices A and B, where  $U_{AB}(\Theta)$  is a shorthand for the matrix  $U_{AB}$  given in (2.19) for  $\mu = \Theta$ . Some algebra involving a repeated use of the same identity (2.32) allows one to prove the more general relation

$$U_{AB}(\Theta - \mu) = S_A U_{AB}(\mu) S_B. \quad (2.34)$$

As a consequence, the Hamiltonians  $\hat{\mathcal{H}}(\mu)$  and  $\hat{\mathcal{H}}(\Theta - \mu)$  have the same spectrum. More precisely, if  $\psi_A$  is an eigenfunction of  $\hat{\mathcal{H}}(\mu)$  with energy  $E$ , (2.34) shows that  $\chi_A = S_A \psi_A$  is an eigenfunction of  $\hat{\mathcal{H}}(\Theta - \mu)$  with the same energy  $E$ .

*Special values of  $\mu$ .* The following two values of the parameter  $\mu$ :

$$\mu_0 = \Theta/2, \quad \mu_1 = \Theta/2 + \pi, \quad (2.35)$$

are special in several respects. The  $\mu \leftrightarrow \Theta - \mu$  symmetry and the semi-periodicity imply that  $\mu_0$  and  $\mu_1$  are symmetry axes of the energy spectrum, if displayed as a function of  $\mu$ . The Kramers degeneracy and the  $\mu \leftrightarrow \Theta - \mu$  symmetry imply that all energy levels are at least fourfold degenerate, i.e., that all the multiplicities are multiples of 4.

There is also a striking correspondence between the present problem at the special value  $\mu_0$  and the tight-binding problem in the presence of a magnetic monopole investigated in [2]. The mapping between both problems goes as follows. For  $\mu = \mu_0 = \Theta/2$  one has

$$2 \cos \mu_0 U_{AB}(\mu_0) = 1 + S_A S_B. \quad (2.36)$$

This formula, which is essentially equivalent to (2.33), suggests to introduce the local basis of eigenstates of the spin operators  $S_A$ . Denoting by  $(\theta_A, \varphi_A)$  the spherical coordinates of A, such that

$$\mathbf{A} = (\sin \theta_A \cos \varphi_A, \sin \theta_A \sin \varphi_A, \cos \theta_A), \quad (2.37)$$

the spinors  $\chi_A^\pm$  such that  $S_A \chi_A^\pm = \pm \chi_A^\pm$  read

$$\chi_A^+ = \begin{pmatrix} \cos \frac{\theta_A}{2} \\ \sin \frac{\theta_A}{2} e^{i\varphi_A} \end{pmatrix}, \quad \chi_A^- = \begin{pmatrix} -\sin \frac{\theta_A}{2} e^{-i\varphi_A} \\ \cos \frac{\theta_A}{2} \end{pmatrix}. \quad (2.38)$$

The spinors  $\chi_A^\pm$  are changed into one another by time-reversal symmetry, according to (2.28). Expanding the eigenfunctions of  $\hat{\mathcal{H}}$  as

$$\psi_A = u_A \chi_A^+ + v_A \chi_A^-, \quad (2.39)$$

some algebra using (2.36) shows that the amplitudes  $u_A$  and  $v_A$  obey the following two scalar tight-binding equations:

$$E u_A = \sum_{B(A)} t_{AB} u_B, \quad E v_A = \sum_{B(A)} t_{AB}^* v_B, \quad (2.40)$$

where the hopping rate  $t_{AB}$  is given by

$$2 \cos \mu_0 t_{AB} = \langle \chi_A^+ | \chi_B^+ \rangle = \cos \frac{\theta_A}{2} \cos \frac{\theta_B}{2} + \sin \frac{\theta_A}{2} \sin \frac{\theta_B}{2} e^{i(\varphi_B - \varphi_A)}. \quad (2.41)$$

The expression (2.41) of  $t_{AB}$  can be drastically simplified as follows. Using trigonometric identities and the relation

$$\cos \Theta = \cos \theta_A \cos \theta_B + \sin \theta_A \sin \theta_B \cos(\varphi_B - \varphi_A), \quad (2.42)$$

the expression for the square modulus of  $t_{AB}$  can be shown to boil down to  $|t_{AB}|^2 = 1$ . The hopping rates are therefore phase factors. Setting  $t_{AB} = \exp(i\omega_{AB})$ , we obtain

$$\cos \omega_{AB} = \frac{\cos \Theta + \cos \theta_A + \cos \theta_B + 1}{4 \cos \frac{\Theta}{2} \cos \frac{\theta_A}{2} \cos \frac{\theta_B}{2}}. \quad (2.43)$$

This expression can be recognized as one of the variants of the spherical Heron formula giving the solid angle of a spherical triangle in terms of its arc lengths [17, 18], recalled in the Appendix of [2]. We thus obtain

$$t_{AB} = \exp\left(\frac{i\Omega_{NAB}}{2}\right), \quad (2.44)$$

where  $\Omega_{NAB}$  is the solid angle of the oriented spherical triangle NAB, where N is the North pole of the unit sphere. It can be checked that phases and orientations are consistent, so that the product of phase factors living on the anticlockwise oriented links around any face equals  $\exp(i\Omega/2)$ , where  $\Omega$  is the spherical angle of the face under consideration. This is precisely the requirement to describe the magnetic flux generated by a magnetic monopole of unit charge ( $n = 1$ ) sitting at the center of the sphere.

We have therefore shown that the spectrum of the present problem at the special value  $\mu = \mu_0 = \Theta/2$  consists of two independent copies of the spectrum of the magnetic monopole problem for  $n = \pm 1$ . One may wonder how the Hamiltonian  $\mathcal{H}$ , which is invariant under time reversal, can have at the special point  $\mu = \mu_0 = \Theta/2$  the same spectrum as the Hamiltonian of the magnetic monopole problem, for which the time-reversal symmetry is broken. The key to the answer is that the expansion (2.39), which is the step that seemingly breaks time-reversal symmetry, amounts to performing a unitary transformation  $\mathcal{D}$  which brings the  $2V \times 2V$  Hamiltonian matrix  $\mathcal{H}$  into the block diagonal form

$$\overline{\mathcal{H}} = \mathcal{D}\mathcal{H}\mathcal{D}^\dagger = \begin{pmatrix} \mathcal{H}_+ & 0 \\ 0 & \mathcal{H}_- \end{pmatrix}, \quad (2.45)$$

where  $\mathcal{H}_\pm$  are the  $V \times V$  Hamiltonian matrices of the magnetic monopole problem with respective magnetic charges  $n = \pm 1$ . The full Hamiltonian  $\overline{\mathcal{H}}$  is invariant under time reversal. The operators  $\mathcal{H}_+$  and  $\mathcal{H}_- = \mathcal{H}_+^\dagger$  separately break time-reversal symmetry, but they are changed into one another by time reversal. Each of them brings one copy of the spectrum of the magnetic monopole problem.

### 3. Polyhedra and their spectra

In this section we investigate the spectrum of the tight-binding Hamiltonian  $\hat{\mathcal{H}}$  for the five regular polyhedra or Platonic solids and for the fullerene, modeled as a symmetric truncated icosahedron. In the case of the Platonic solids, all the properties derived in

Section 2.2 will be checked against our analytic expressions of the energy spectra. The fullerene will be special in the following two respects. Its energy spectrum will not be obtained analytically, albeit from the numerical diagonalization of an explicit  $120 \times 120$  matrix. The homogeneous modes described in Section 2.2 are absent, as the fullerene is not sufficiently symmetric to allow them.

All these polyhedra have been described in detail in [2]. Table 1 lists a few of their geometrical characteristics which will be useful in the following.

polyhedron	$V$	$L$	$F$	$p$	$q$	$\cos \Theta$
tetrahedron	4	6	4	3	3	$-1/3$
cube	8	12	6	3	4	$1/3$
octahedron	6	12	8	4	3	0
dodecahedron	20	30	12	3	5	$\sqrt{5}/3$
icosahedron	12	30	20	5	3	$\sqrt{5}/5$
fullerene	60	90	32	3	$\begin{cases} 5 \\ 6 \end{cases}$	$(80 + 9\sqrt{5})/109$

**Table 1.** Geometrical characteristics of the polyhedra considered in this work: numbers  $V$  of vertices,  $L$  of links,  $F$  of faces, coordination number (number of neighbors of a vertex)  $p$ , number of sides of a face  $q$ , expression of  $\cos \Theta$ , where the arc length  $\Theta$  of the links has been introduced in (2.2).

### 3.1. The tetrahedron

The tetrahedron is the simplest of the Platonic solids. It consists of 4 trivalent vertices, 6 links and 4 triangular faces.

Throughout the following it will be advantageous to unwrap the polyhedra around an axis of high symmetry, say of order  $r$ , to be used as the  $z$ -axis [19]. For all the Platonic solids, the order  $r$  of rotational symmetry can be chosen to be the larger of the integers  $p$  and  $q$ . The planar representation of the tetrahedron thus obtained, emphasizing the vertices and the links between them, is shown in Figure 1. Some vertices and links may have several occurrences, to be identified by the inverse procedure of wrapping the planar representation onto the sphere. This planar representation is an efficient tool to find the Cartesian coordinates of the vertices, making an optimal use of symmetries. Vertices at the same height on the plot have the same  $z$  coordinate, whereas their coordinates in the  $xy$ -plane are obtained from each other by rotations by the commensurate angles  $2\pi k/r$  for  $k = 1, \dots, r$ . Table 2 lists the coordinates of the vertices thus obtained.

The  $8 \times 8$  Hamiltonian matrix  $\mathcal{H}$  has been constructed from these coordinates by using (2.19) and (2.24). This matrix is too complex to be diagonalizable by hand. For each of the five Platonic solids this task has been performed with the help of the software MACSYMA. The energy eigenvalues and their multiplicities are listed in Table 3. Horizontal lines separate groups of levels related to each other by the

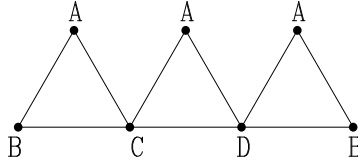


**Figure 1.** Planar representation of the tetrahedron.

vertex	$x$	$y$	$z$
A	0	0	1
B	$2\sqrt{2}/3$	0	$-1/3$
C	$-\sqrt{2}/3$	$\sqrt{6}/3$	$-1/3$
D	$-\sqrt{2}/3$	$-\sqrt{6}/3$	$-1/3$

**Table 2.** Cartesian coordinates of the vertices of the tetrahedron. Horizontal lines separate groups of vertices having the same  $z$  coordinate.

$\mu \leftrightarrow \Theta - \mu$  symmetry. The levels  $E_1(\mu)$  and  $E_2(\mu)$  are interchanged by this symmetry, whereas  $E_3(\mu)$  is symmetric by itself. One has indeed

$$E_2(\mu) = E_1(\Theta - \mu), \quad E_3(\mu) = -\sqrt{3} \cos(\mu - \Theta/2). \quad (3.1)$$

The energy spectrum is shown in Figure 2 as a function of  $\mu/(2\pi)$  over one period. The vertical dashed lines show the symmetry axes of the spectrum at the special values of  $\mu$  given in (2.35).

$a$	$E_a(\mu)$	$m_a$
1	$3 \cos \mu$	2
2	$-\cos \mu + 2\sqrt{2} \sin \mu$	2
3	$-\cos \mu - \sqrt{2} \sin \mu$	4

**Table 3.** Energy levels  $E_a(\mu)$  of the tetrahedron and their multiplicities  $m_a$ . Horizontal lines separate groups of levels related to each other by the  $\mu \leftrightarrow \Theta - \mu$  symmetry.

### 3.2. The cube

The planar representation of the cube is shown in Figure 3. Table 4 lists the Cartesian coordinates of the vertices.

The energy eigenvalues of the  $16 \times 16$  Hamiltonian matrix constructed from these coordinates are listed in Table 5 and shown in Figure 4 as a function of  $\mu/(2\pi)$  over one period. The spectrum is observed to be its own opposite, i.e., to be symmetric with respect to the origin of energies,  $E = 0$ . This extra symmetry is particular to the cube, being due to the fact that this polyhedron is *bipartite*.

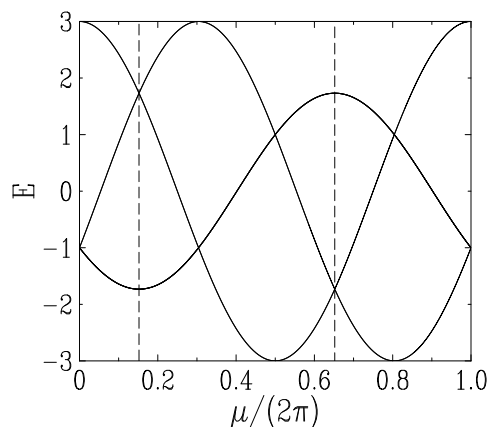


**Figure 2.** Plot of the energy spectrum of the tetrahedron against  $\mu/(2\pi)$  over one period. Vertical dashed lines: symmetry axes at the special values of  $\mu$  given in (2.35).

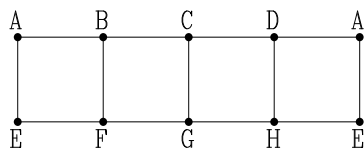


**Figure 3.** Planar representation of the cube.

vertex	$x$	$y$	$z$
A	$1/\sqrt{3}$	$1/\sqrt{3}$	$1/\sqrt{3}$
B	$-1/\sqrt{3}$	$1/\sqrt{3}$	$1/\sqrt{3}$
C	$-1/\sqrt{3}$	$-1/\sqrt{3}$	$1/\sqrt{3}$
D	$1/\sqrt{3}$	$-1/\sqrt{3}$	$1/\sqrt{3}$
E	$1/\sqrt{3}$	$1/\sqrt{3}$	$-1/\sqrt{3}$
F	$-1/\sqrt{3}$	$1/\sqrt{3}$	$-1/\sqrt{3}$
G	$-1/\sqrt{3}$	$-1/\sqrt{3}$	$-1/\sqrt{3}$
H	$1/\sqrt{3}$	$-1/\sqrt{3}$	$-1/\sqrt{3}$

**Table 4.** Cartesian coordinates of the vertices of the cube. Same conventions as in Table 2.

### 3.3. The octahedron

The planar representation of the octahedron is shown in Figure 5. Table 6 lists the Cartesian coordinates of the vertices.

The energy eigenvalues of the  $12 \times 12$  Hamiltonian matrix constructed from these coordinates are listed in Table 7 and shown in Figure 6 as a function of  $\mu/(2\pi)$  over one period.

$a$	$E_a(\mu)$	$m_a$
1	$3 \cos \mu$	2
2	$\cos \mu + 2\sqrt{2} \sin \mu$	2
3	$\cos \mu - \sqrt{2} \sin \mu$	4
4	$-\cos \mu + \sqrt{2} \sin \mu$	4
5	$-\cos \mu - 2\sqrt{2} \sin \mu$	2
6	$-3 \cos \mu$	2

**Table 5.** Energy levels  $E_a(\mu)$  of the cube and their multiplicities  $m_a$ . Same conventions as in Table 3.

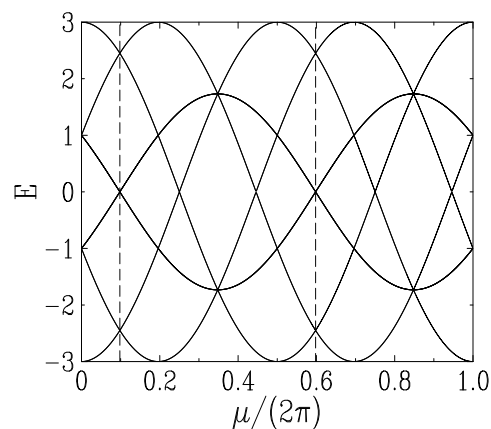


**Figure 4.** Plot of the energy spectrum of the cube against  $\mu/(2\pi)$  over one period. Same conventions as in Figure 2.

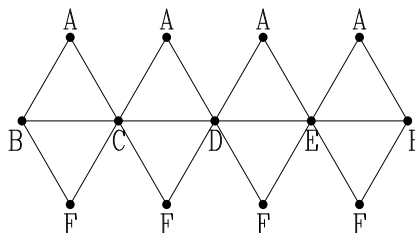


**Figure 5.** Planar representation of the octahedron.

### 3.4. The dodecahedron

The planar representation of the dodecahedron is shown in Figure 7. Table 8 lists the Cartesian coordinates of the vertices, with the shorthand notations  $c_k = \cos(k\pi/5)$ ,  $s_k = \sin(k\pi/5)$ , and

$$\begin{aligned}
 a &= \sqrt{\frac{2(5 - \sqrt{5})}{15}}, & a' &= \sqrt{\frac{5 + 2\sqrt{5}}{15}}, \\
 b &= \sqrt{\frac{2(5 + \sqrt{5})}{15}}, & b' &= \sqrt{\frac{5 - 2\sqrt{5}}{15}}.
 \end{aligned} \tag{3.2}$$

vertex	$x$	$y$	$z$
A	0	0	1
B	1	0	0
C	0	1	0
D	-1	0	0
E	0	-1	0
F	0	0	-1

**Table 6.** Cartesian coordinates of the vertices of the octahedron. Same conventions as in Table 2.

$a$	$E_a(\mu)$	$m_a$
1	$4 \cos \mu$	2
2	$4 \sin \mu$	2
3	$-2 \sin \mu$	4
4	$-2 \cos \mu$	4

**Table 7.** Energy levels  $E_a(\mu)$  of the octahedron and their multiplicities  $m_a$ . Same conventions as in Table 3.

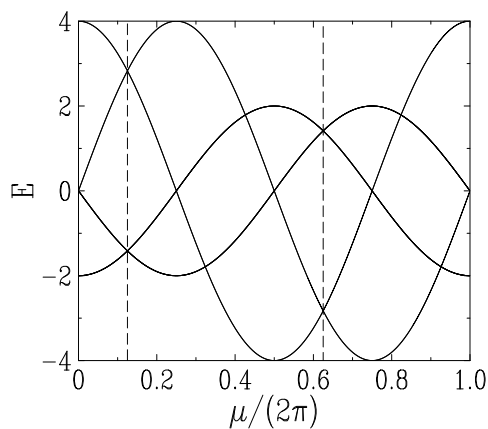


**Figure 6.** Plot of the energy spectrum of the octahedron against  $\mu/(2\pi)$  over one period. Same conventions as in Figure 2.

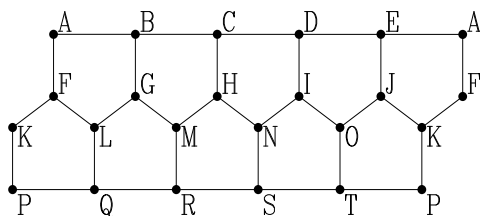


**Figure 7.** Planar representation of the dodecahedron.

The energy eigenvalues of the  $40 \times 40$  Hamiltonian matrix constructed from these

vertex	$x$	$y$	$z$	vertex	$x$	$y$	$z$
A	$a c_0$	$a s_0$	$a'$	K	$b c_9$	$b s_9$	$-b'$
B	$a c_2$	$a s_2$	$a'$	L	$b c_1$	$b s_1$	$-b'$
C	$a c_4$	$a s_4$	$a'$	M	$b c_3$	$b s_3$	$-b'$
D	$a c_6$	$a s_6$	$a'$	N	$b c_5$	$b s_5$	$-b'$
E	$a c_8$	$a s_8$	$a'$	O	$b c_7$	$b s_7$	$-b'$
F	$b c_0$	$b s_0$	$b'$	P	$a c_9$	$a s_9$	$-a'$
G	$b c_2$	$b s_2$	$b'$	Q	$a c_1$	$a s_1$	$-a'$
H	$b c_4$	$b s_4$	$b'$	R	$a c_3$	$a s_3$	$-a'$
I	$b c_6$	$b s_6$	$b'$	S	$a c_5$	$a s_5$	$-a'$
J	$b c_8$	$b s_8$	$b'$	T	$a c_7$	$a s_7$	$-a'$

**Table 8.** Cartesian coordinates of the vertices of the dodecahedron. Same conventions as in Table 2. Shorthand notations are explained in and above (3.2).

coordinates are listed in Table 9 and shown in Figure 8 as a function of  $\mu/(2\pi)$  over one period. This is the first example where some of the energy levels are not given by linear functions of  $\cos \mu$  and  $\sin \mu$ . The four sixfold degenerate energy levels  $\varepsilon_i(\mu)$  ( $i = 1, 2, 3, 4$ ) are the roots of the polynomial equation

$$\varepsilon^4 + 2\xi\varepsilon^3 + (2\xi^2 - 5)\varepsilon^2 + 2\xi(\xi^2 - 4)\varepsilon + 1 - 3\xi^2 + \xi^4 = 0, \quad (3.3)$$

with

$$\xi = \frac{\sqrt{5} + 1}{2} \cos \mu + \frac{\sqrt{5} - 1}{2} \sin \mu = \sqrt{3} \cos(\mu - \Theta/2), \quad (3.4)$$

and where the branches are chosen such that  $\varepsilon_1(0) = 1$ ,  $\varepsilon_2(0) = 0$ ,  $\varepsilon_3(0) = -2$ ,  $\varepsilon_4(0) = -\sqrt{5}$ .

$a$	$E_a(\mu)$	$m_a$
1	$3 \cos \mu$	2
2	$\sqrt{5} \cos \mu + 2 \sin \mu$	2
3	$\sqrt{5} \cos \mu - \sin \mu$	4
4	$\cos \mu + \sqrt{5} \sin \mu$	4
5	$\varepsilon_1(\mu)$	6
6	$\varepsilon_2(\mu)$	6
7	$-3 \sin \mu$	2
8	$-2 \cos \mu + \sqrt{5} \sin \mu$	2
9	$\varepsilon_3(\mu)$	6
10	$\varepsilon_4(\mu)$	6

**Table 9.** Energy levels  $E_a(\mu)$  of the dodecahedron and their multiplicities  $m_a$ . Same conventions as in Table 3. The functions  $\varepsilon_i(\mu)$  ( $i = 1, 2, 3, 4$ ) are the roots of the polynomial equation (3.3).

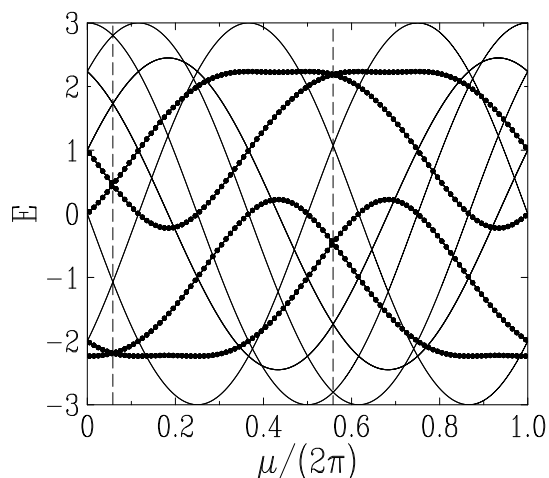


**Figure 8.** Plot of the energy spectrum of the dodecahedron against  $\mu/(2\pi)$  over one period. Same conventions as in Figure 2. Thick dotted lines: sixfold degenerate energy levels  $\varepsilon_i(\mu)$  ( $i = 1, 2, 3, 4$ ).

### 3.5. The icosahedron

The planar representation of the icosahedron is shown in Figure 9. Table 10 lists the Cartesian coordinates of the vertices, with the shorthand notations  $c_k = \cos(k\pi/5)$ ,  $s_k = \sin(k\pi/5)$ , and

$$d = \frac{2\sqrt{5}}{5}, \quad d' = \frac{\sqrt{5}}{5}. \quad (3.5)$$

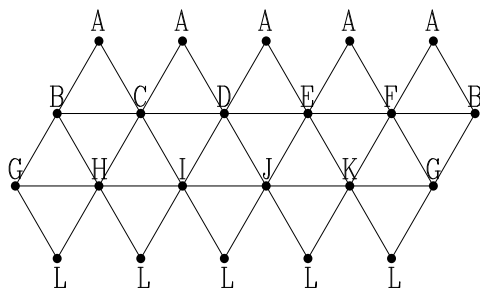


**Figure 9.** Planar representation of the icosahedron.

The energy eigenvalues of the  $24 \times 24$  Hamiltonian matrix constructed from these coordinates are listed in Table 11 and shown in Figure 10 as a function of  $\mu/(2\pi)$  over one period.

### 3.6. The fullerene

We now turn to the case of the  $C_{60}$  fullerene. For simplicity we model this molecule as a symmetric truncated icosahedron, where all the links have equal lengths, so that the analysis of Section 2.1 applies. Let us however recall that this symmetry is known to be

vertex	$x$	$y$	$z$	vertex	$x$	$y$	$z$
A	0	0	1	G	$dc_9$	$ds_9$	$-d'$
B	$dc_0$	$ds_0$	$d'$	H	$dc_1$	$ds_1$	$-d'$
C	$dc_2$	$ds_2$	$d'$	I	$dc_3$	$ds_3$	$-d'$
D	$dc_4$	$ds_4$	$d'$	J	$dc_5$	$ds_5$	$-d'$
E	$dc_6$	$ds_6$	$d'$	K	$dc_7$	$ds_7$	$-d'$
F	$dc_8$	$ds_8$	$d'$	L	0	0	$-1$

**Table 10.** Cartesian coordinates of the vertices of the icosahedron. Same conventions as in Table 2. Shorthand notations are explained in and above (3.5).

$a$	$E_a(\mu)$	$m_a$
1	$5 \cos \mu$	2
2	$\sqrt{5}(\cos \mu + 2 \sin \mu)$	2
3	$\sqrt{5}(\cos \mu - \sin \mu)$	4
4	$-\cos \mu + 3 \sin \mu$	4
5	$-\cos \mu - 2 \sin \mu$	6
6	$-\sqrt{5} \cos \mu$	6

**Table 11.** Energy levels  $E_a(\mu)$  of the icosahedron and their multiplicities  $m_a$ . Same conventions as in Table 3.

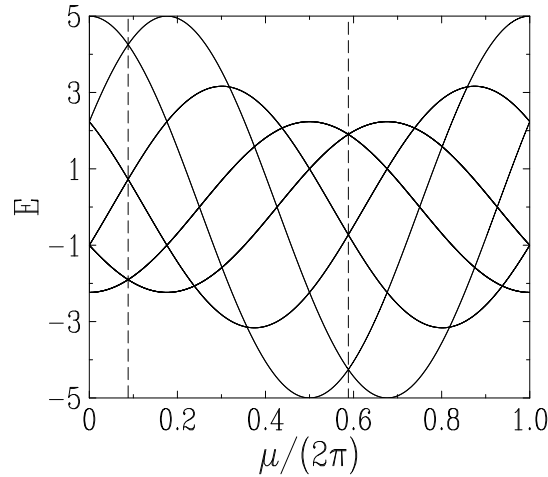


**Figure 10.** Plot of the energy spectrum of the icosahedron against  $\mu/(2\pi)$  over one period. Same conventions as in Figure 2.

slightly violated [20], as for the free molecule the length of the sides of the pentagons is  $1.46 \text{ \AA}$ , whereas the length of the other links is  $1.40 \text{ \AA}$ .

The symmetric truncated icosahedron has  $V = 60$  equivalent vertices,  $L = 90$  equivalent links, and  $F = 32$  faces, namely 12 pentagons and 20 hexagons, respectively corresponding to the vertices and to the faces of the icosahedron. Figure 11 shows the

planar representation obtained by unwrapping the fullerene around a fivefold axis going through the opposite pentagonal faces  $A_1 \dots A_5$  and  $L_1 \dots L_5$ .

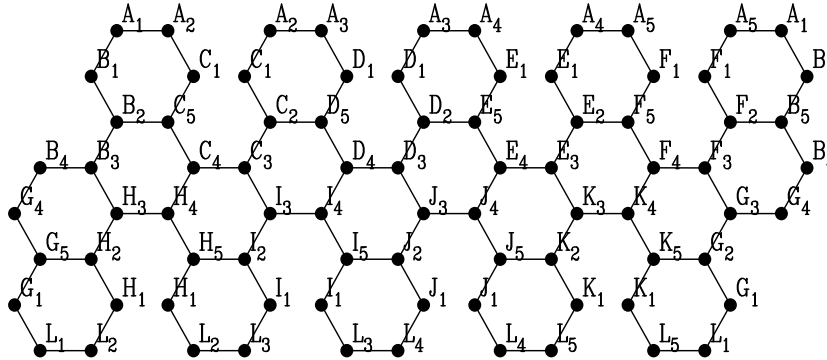


**Figure 11.** Planar representation of the fullerene (symmetric truncated icosahedron).

The Cartesian coordinates of the vertices of the fullerene have been derived from those of the vertices of the icosahedron, listed in Table 10, using the approach described in the Appendix of [2]. This procedure is illustrated in Figure 12, showing an enlargement of the upper left part of Figures 9 and 11, with consistent notations. One has

$$\mathbf{A}_1 = \lambda(2\mathbf{A} + \mathbf{B}), \quad \mathbf{A}_2 = \lambda(2\mathbf{A} + \mathbf{C}), \quad (3.6)$$

and so on, with

$$\lambda = \sqrt{\frac{25 - 4\sqrt{5}}{109}}, \quad (3.7)$$

so that

$$\cos \Theta = \mathbf{A}_1 \cdot \mathbf{A}_2 = (4 + \sqrt{5})\lambda^2 = \frac{80 + 9\sqrt{5}}{109}. \quad (3.8)$$

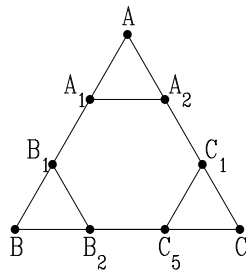


**Figure 12.** The triangular face  $ABC$  of the icosahedron decorated by vertices of the fullerene. Notations are consistent with Figures 9 and 11.

The energy eigenvalues of the  $120 \times 120$  Hamiltonian matrix constructed from the coordinates thus obtained have been evaluated by means of a numerical diagonalization. The energy spectrum is shown in Figure 13 as a function of  $\mu/(2\pi)$  over one period.

For  $\mu = 0$ , i.e., in the absence of spin-orbit coupling, we recover two independent copies of the known tight-binding spectrum of the fullerene [21], with its 15 distinct energy levels with multiplicities ranging from 1 to 9. For generic non-zero values of  $\mu$ , the spectrum consists of 28 distinct energy levels with multiplicities ranging from 2 to 6 only. As  $\mu \rightarrow 0$  the 28 levels merge into the 15 ones according to the patterns given in Table 12. We have introduced the shorthand notation

$$w_{\pm} = \sqrt{2(19 \pm \sqrt{5})}. \quad (3.9)$$

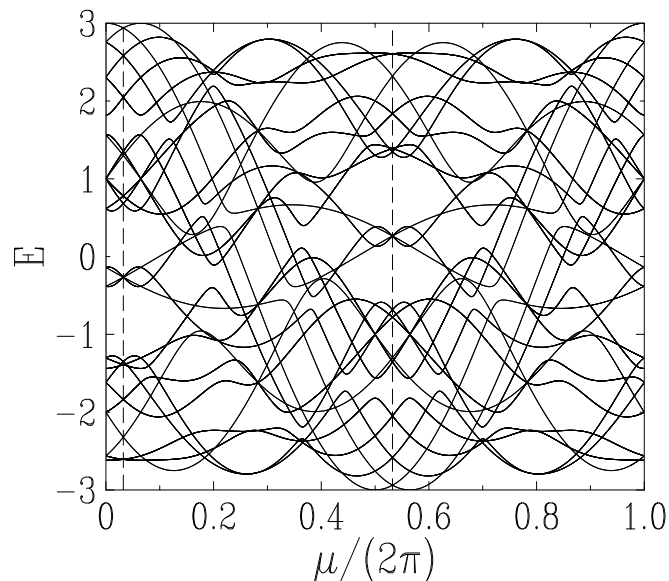


**Figure 13.** Plot of the energy spectrum of the fullerene against  $\mu/(2\pi)$  over one period. Same conventions as in Figure 2.

#### 4. Total energy

An interesting illustration of the above energy spectra is provided by the total energy at half filling, defined as

$$\mathcal{E} = \sum_{a=1}^V E_a, \quad (4.1)$$

where the  $2V$  energy levels are assumed to be in increasing order ( $E_1 \leq E_2 \leq \dots \leq E_{2V}$ ) and repeated according to their multiplicities.

The first of the sum rules (2.27) implies that the total energy thus defined is insensitive to the sign of the Hamiltonian  $\hat{\mathcal{H}}$ . Combining this feature with the symmetries derived in Section 2.2, we conclude that  $\mathcal{E}(\mu)$  obeys the symmetries

$$\mathcal{E}(\mu) = \mathcal{E}(\Theta - \mu) = \mathcal{E}(\mu + \pi). \quad (4.2)$$

The total energy therefore has period  $\pi$ , and exhibits two inequivalent stationary points per period, at

$$\mu_0 = \Theta/2, \quad \mu_m = (\Theta + \pi)/2. \quad (4.3)$$

$E(0)$	$E(0)_{\text{num}}$	$m(0)$	$m(\mu \rightarrow 0)$
3	3	2	2
$(3 + \sqrt{5} + w_-)/4$	2.756598	6	2 + 4
$(\sqrt{13} + 1)/2$	2.302776	10	4 + 6
$(3 - \sqrt{5} + w_+)/4$	1.820249	6	6
$(\sqrt{17} - 1)/2$	1.561553	8	6 + 2
1	1	18	6 + 2 + 6 + 4
$(\sqrt{5} - 1)/2$	0.618034	10	6 + 4
$(3 + \sqrt{5} - w_-)/4$	-0.138564	6	4 + 2
$(\sqrt{5} - 3)/2$	-0.381966	6	2 + 4
$-(\sqrt{13} - 1)/2$	-1.302776	10	4 + 6
$(3 - \sqrt{5} - w_+)/4$	-1.438283	6	6
$-(\sqrt{5} + 1)/2$	-1.618034	10	4 + 6
-2	-2	8	6 + 2
$-(\sqrt{17} + 1)/2$	-2.561553	8	2 + 6
$-(\sqrt{5} + 3)/2$	-2.618034	6	6

**Table 12.** Energy levels  $E(0)$  of the fullerene at  $\mu = 0$ , with their multiplicities  $m(0)$  and degeneracy-lifting patterns at small  $\mu \neq 0$ . The shorthand notation  $w_{\pm}$  has been introduced in (3.9).

The first of these values,  $\mu_0$ , coincides with one of the special values introduced in (2.35), i.e., one of the symmetry axes of the spectrum. The second of the above values,  $\mu_m$ , corresponds to one of the midpoints between the latter symmetry axes.

The second of the sum rules (2.27) implies that the mean squared value of the individual energy levels is  $\langle E^2 \rangle = 4L/(2V) = p$ , where  $p$  is the coordination number of the vertices. This suggests to introduce the reduced total energy

$$\mathcal{E}_r = \frac{\mathcal{E}}{2V\sqrt{\langle E^2 \rangle}} = \frac{\mathcal{E}}{2V\sqrt{p}} = \frac{\mathcal{E}}{2\sqrt{2VL}}. \quad (4.4)$$

This heuristic argument can be turned to a quantitative prediction in the  $p \rightarrow \infty$  limit of a very highly connected structure [2]. In this limit, the reduced total energy  $\mathcal{E}_r$  has been shown to have the universal limiting value

$$\mathcal{E}_{\infty} = -\frac{1}{\sqrt{2\pi}} = -0.398942. \quad (4.5)$$

Figure 14 shows a plot of the reduced total energy  $\mathcal{E}_r$  for all the polyhedra investigated in this work, as a function of  $(\mu - \mu_0)/\pi$  over one period. The reduced total energy is observed to wander around the limiting value (4.5), shown as a dashed line. The amplitude of the oscillations, i.e., of the dependence of the total energy on the parameter  $\mu$ , is a decreasing function of the number of vertices. Figure 15 shows an enlargement of the plot focusing on the weak  $\mu$ -dependence of  $\mathcal{E}_r$  in the two examples with the larger numbers of vertices, i.e., the dodecahedron ( $V = 20$ ) and the fullerene

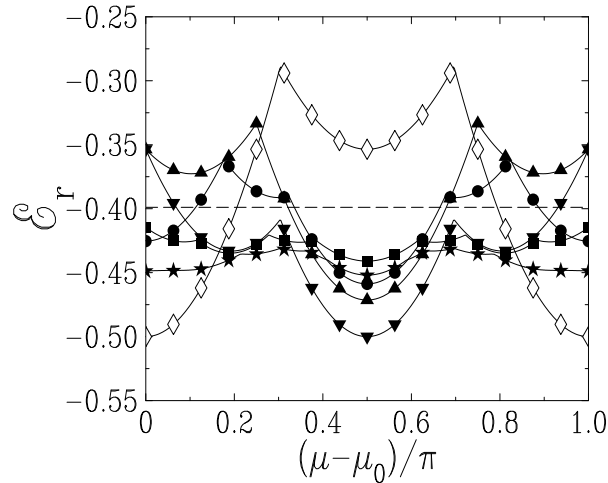


**Figure 14.** Plot of the reduced total energy  $\mathcal{E}_r$  against  $(\mu - \mu_0)/\pi$ , for all the polyhedra investigated in this work: tetrahedron ( $V = 4$ ) (empty diamonds), cube ( $V = 8$ ) (down triangles), octahedron ( $V = 6$ ) (up triangles), dodecahedron ( $V = 20$ ) (squares), icosahedron ( $V = 12$ ) (circles) and fullerene ( $V = 60$ ) (stars). The curves consist of many more points than symbols (500 data points for each polyhedron). The horizontal dashed line shows the limiting value (4.5).

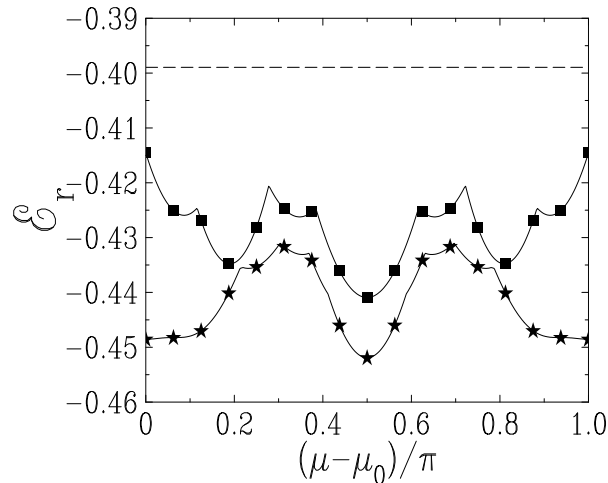


**Figure 15.** Enlargement of Figure 14, with the same conventions, emphasizing the weak  $\mu$ -dependence of the reduced total energy  $\mathcal{E}_r$  in the cases of the dodecahedron and of the fullerene.

( $V = 60$ ). The abscissa axes in Figures 14 and 15 are such that the stationary point  $\mu_0$  introduced in (4.3) corresponds to the ends of the plots, whereas  $\mu_m$  corresponds to their centers. The latter stationary point is observed to be the absolute minimum of the total energy for all the polyhedra considered in this work, except the tetrahedron, for which the total energy has its absolute minimum at  $\mu = \mu_0$  and a local minimum at  $\mu = \mu_m$ .

## 5. Discussion

In this paper we have introduced and investigated a tight-binding model defined on graphs drawn on the unit sphere, describing the motion of an electron subject to a spin-orbit interaction in the radial electric field created by a classical charge sitting at the center of the sphere. The present work completes our study of electronic properties of mesoscopic and nanoscopic systems with the topology of the sphere, started in the companion work [2], which is devoted to electrons subject to a radial magnetic field produced by a quantized magnetic charge sitting at the center of the sphere.

This work has been focused onto polyhedral graphs such that all links have a common arc length  $\Theta$ . For a fixed graph of this kind, the model has only one parameter,  $\mu$ , giving a dimensionless measure of the strength of the spin-orbit interaction. Among the symmetry properties of the model, exposed in detail in Section 2.2, the  $\mu \leftrightarrow \Theta - \mu$  symmetry was quite unexpected, as it has no counterpart in the continuum, described by the familiar form  $\mathbf{L} \cdot \mathbf{S}$  of the spin-orbit Hamiltonian, whose eigenvalues and multiplicities are recalled in (1.6).

For the special value  $\mu = \mu_0 = \Theta/2$ , which coincides with one of the symmetry axes of the spectra, an exact correspondence has been established with the tight-binding problem in the magnetic field of a Dirac monopole, investigated in [2]. It is remarkable that, by tuning a parameter in a theory which is experimentally realizable, it is possible to obtain the spectrum of another system whose experimental realization is so far elusive. In fact this correspondence already holds at the classical level. It was indeed discovered long ago by Poincaré [22] that the motion of an electrically charged particle in the field of a magnetic charge can be mapped onto that of a spherical top. In a quantum-mechanical framework, the quantitative correspondence between both problems reads [23, 24]

$$|n| = 2S, \tag{5.1}$$

where the integer  $n$  is the magnetic charge (in units of the elementary magnetic charge of Dirac's monopole), whereas  $S$  is the total spin of the top. The above relation can easily be recovered by noticing that the ground state of the Schrödinger equation on the sphere in the presence of a magnetic charge  $n$ , investigated in the pioneering work of Tamm [25], has a multiplicity  $|n| + 1$ , to be identified with  $2S + 1$ . In the present situation of an electron ( $S = 1/2$ ), the correspondence has indeed been shown to hold for a unit magnetic charge ( $n = \pm 1$ ). More generally, a similar correspondence can be expected to hold true for higher representations as well, whenever the spin and the magnetic charge are related by (5.1), for a suitably chosen special form of the spin-orbit interaction.

We have then turned to the study of specific examples of polyhedra, namely the five Platonic solids (tetrahedron, cube, octahedron, dodecahedron and icosahedron) and the  $C_{60}$  fullerene (modeled as a regular truncated icosahedron). For the Platonic solids, the full  $\mu$ -dependence of the energy levels, and the corresponding multiplicities, have been obtained analytically in Sections 3.1–3.5. These results allow for an explicit check of the general properties listed in Section 2.2. Rather surprisingly, all the energy levels can be

expressed as linear combinations of  $\sin \mu$  and  $\cos \mu$ , except the four sixfold degenerate levels of the dodecahedron, which are obtained as the roots of a fourth-degree polynomial given in (3.3). This simplicity of the energy eigenvalues is to be contrasted with the rather large dimension,  $2V$ , of the Hamiltonian matrices, i.e., 40 for the dodecahedron.

Pursuing along the lines of our companion work [2], we have also evaluated the total electronic energy  $\mathcal{E}$  of the system at half filling. For all the examples considered in this work, this total energy is found to be rather close to its asymptotic value in the limit of large coordination numbers, where the density of states becomes Gaussian. Finally, as far as its dependence on the parameter  $\mu$  is concerned, the total energy reaches its absolute minima at the midpoints between the symmetry axes of the spectra for all the polyhedra considered in this work, except for the tetrahedron where the total energy has its absolute minima at the symmetry axes of the spectrum and local minima at the midpoints.

### Acknowledgments

It is a pleasure for us to thank B. Douçot, G. Montambaux and O. Entin-Wohlman for very stimulating discussions.

### References

- [1] Imry Y, 2002 *Introduction to Mesoscopic Physics* 2nd ed (Oxford: Oxford University Press)
- [2] Avishai Y and Luck J M, 2008 *Tight-binding electronic spectra on graphs with spherical topology I: the effect of a magnetic charge* Preprint arXiv:0801.1460
- [3] Rashba E I, 1960 *Sov. Phys. Solid State* **2** 1109  
Bychkov Y A and Rashba E I, 1984 *Sov. Phys. JETP Lett.* **39** 78
- [4] Hikami S, Larkin A I and Nagaoka Y, 1980 *Prog. Theor. Phys.* **63** 707  
Ando T, 1989 *Phys. Rev. B* **40** 5325
- [5] Berestetskii V B, Lifshitz E M and Pitaevskii L P, 1971 *Relativistic Quantum Theory* (Oxford: Pergamon)
- [6] Goldberger M L and Watson K M, 1964 *Collision Theory* (New York: Wiley)
- [7] Peierls R E, 1933 *Z. Phys.* **80** 763  
Luttinger J M, 1951 *Phys. Rev.* **84** 814  
Kohn W, 1959 *Phys. Rev.* **115** 1460
- [8] Graf M and Vogt P, 1995 *Phys. Rev. B* **51** 4940
- [9] Boykin T B, Bowen R C and Klimeck G, 2001 *Phys. Rev. B* **63** 245314  
Boykin T B, 2001 *Am. J. Phys.* **69** 793
- [10] Wilson R J, 1979 *Introduction to Graph Theory* 2nd ed (London: Longman)
- [11] Fröhlich J and Studer U M, 1993 *Rev. Mod. Phys.* **65** 733
- [12] Shahbazyan T V and Raikh M E, 1994 *Phys. Rev. Lett.* **73** 1408
- [13] Entin-Wohlman O, Aharony A, Galperin Y M, Kozub V I and Vinokur V, 2005 *Phys. Rev. Lett.* **95** 086603
- [14] Engel H A, Rashba E I and Halperin B I, 2007 *Theory of Spin Hall Effects in Semiconductors* in *Handbook of Magnetism and Advanced Magnetic Materials* 2858-2877 Kronmüller H and Parkin S eds (Chichester, UK: Wiley) Preprint arXiv:cond-mat/0603306
- [15] Kramers H A, 1930 *Proc. Acad. Amsterdam* **33** 959
- [16] Landau L D and Lifshitz E M, 1959 *Quantum Mechanics* (London: Pergamon)

- [17] Korn G A and Korn T M, 1968 *Mathematical Handbook for Scientists and Engineers* (New York: McGraw-Hill)
- [18] Ito K ed, 1980 *The Encyclopedic Dictionary of Mathematics* 2nd ed (Cambridge, MA: MIT Press)
- [19] Sadoc J F and Mosseri R, 1999 *Geometrical Frustration* Monographs and Texts in Statistical Physics (New York: Cambridge University Press)
- [20] Hedberg K, Hedberg L, Bethune D S, Brown C A, Dorn H C, Johnson R D and Devries M, 1991 *Science* **254** 410
- [21] Manousakis E, 1991 *Phys. Rev. B* **44** 10991
- [22] Poincaré H, 1896 *C.R. Acad. Sci. Paris* **123** 350
- [23] Haldane F D M, 1983 *Phys. Rev. Lett.* **51** 605
- [24] Shnir Y, 2005 *Magnetic Monopoles* (Berlin: Springer)
- [25] Tamm I, 1931 *Z. Phys.* **71** 141